Thermal Aspects in the Continuous Chemical Vapor Deposition of Silicon

Hoseon Yoo
Department of Mechanical Engineering,
Soongsil University,
Seoul 156-743, Korea

Yogesh Jaluria
Fellow ASME
e-mail: jaluria@jove.rutgers.edu
Department of Mechanical
and Aerospace Engineering,
Rutgers, The State University of New Jersey,
New Brunswick, NJ 08854

This paper deals with the continuous chemical vapor deposition of silicon in a horizontal cold wall reactor, paying special attention to a moving susceptor. A two-dimensional numerical model, which accounts for variable properties, thermal diffusion, radiative heat exchange among surfaces, and conjugate heat transfer between the gas and susceptor, is developed and validated. Scale analysis for the susceptor energy balance enables the identification of the characteristic parameters and the prediction of their qualitative effects before carrying out a detailed analysis. The results from the scale analysis are found to be consistent with the numerical predictions. The results show that the present continuous system is characterized by two newly defined parameters: conductance ratio and susceptor parameter. A pair of performance curves that relate the deposition efficiency to each parameter successfully provide the susceptor-related design conditions. It is also revealed that there exists an optimum length of heating zone that maximizes the deposition efficiency. [DOI: 10.1115/1.1482084]

Keywords: Conjugate, Heat Transfer, Mass Transfer, Radiation, Thin Films, Vapor Deposition

Introduction

Chemical vapor deposition (CVD) is an important method for manufacturing thin films. Since thin films prepared by CVD have many attractive features, such as large area coverage, good control of film structure and composition, and conformal deposition, the technology is being employed in a variety of areas. Engineering applications include the fabrication of microelectronic circuits, wear- and corrosion-resistant coatings, recording media, solar cells, and optical devices. In view of ever increasing demands on the deposition performance, one of the most important issues in the future CVD technology is the productivity. The requirement of higher throughputs necessitates new or refined designs in CVD systems.

From the viewpoint of processing, most of the previous studies on CVD have dealt with batch systems, where a limited number of substrates or wafers placed on a stationary or rotating susceptor are processed at one time. A number of existing reactors that have evolved to meet the requirements, especially deposition uniformity, arising from various applications belong to the same category. Research efforts for modeling transport phenomena occurring in these reactors and chemical reactions involved in deposition processes have been reviewed by Jensen et al. [1], Kleijn [2], and Mahajan [3]. The productivity of batch processing is essentially limited by downtime associated with product loading, reactor startup, and shutdown.

One of the ways to improve production throughput in CVD systems is to adopt continuous processing. The feasibility and utility of continuous processing have been exploited in a number of industrial applications. Yamaji et al. [4] reported that their continuous CVD siliconizing line succeeded in the manufacture of a silicon-coated steel sheet. Stevenson and Matthews [5] suggested design criteria for continuous processing of a plasma-assisted physical vapor deposition (PVD) equipment through cost analysis. Onabe et al. [6] prepared superconducting tapes using a continuous CVD technique. In addition, continuous CVD processing has been actively applied to coatings of glass [7] and fiber [8,9]. These works have addressed experimental conditions, film properties, conceptual designs, or equipment development, but have lacked detailed descriptions of processes and transport phenomena occurring in the reactor, that are needed for appropriate understanding and modeling of continuous systems.

Recently, Chiu and Jaluria [10,11] have proposed two types of continuous CVD systems based on a horizontal reactor, modeled deposition processes, and assessed their feasibility as alternatives to batch processing. One of these systems, where a finite thickness susceptor moves along the reactor bottom wall in a straight channel horizontal reactor [11], is somewhat simpler and more flexible. Such a layout allows for uninterrupted operation, precluding the concern with downtime. Moreover, film uniformity is not of primary concern since the susceptor moving at a constant speed, under steady state, experiences the same amount of deposition over the entire reactor length. This system resembles practically used injector-based atmospheric CVD reactor [12,13] in that they commonly adopt a moving susceptor, on which wafers are continuously and compactly placed, to achieve uniform deposition and high throughput. Although some basic aspects have already been presented, the continuous system needs to be revisited for better understanding of its nature and for obtaining the performance characteristics applicable to design. In addition, the effects of conjugate heat transfer and susceptor motion need to be quantified.

Motivated by such necessity, the present study considers the same continuous system as the previous work [11]. The prospect of its adoption in the practical process seems to be encouraging since it is simpler in layout than the injector-based reactor mentioned earlier. We investigate transport phenomena and chemical reactions accompanying the deposition process while paying special attention to the moving susceptor. The numerical model encompasses variable properties, thermal diffusion, radiative exchange among surfaces, and conjugate heat transfer between the gas phase and moving solid susceptor. A useful feature of this work lies in the use of scale analysis, as complementary to the numerical simulation, in identifying the characteristic parameters and analyzing the predicted results. In order to represent the performance of continuous CVD processing, a deposition efficiency is defined and interpreted. The characteristics and importance of

Contributed by the Heat Transfer Division for publication in the JOURNAL OF HEAT TRANSFER. Manuscript received by the Heat Transfer Division August 17, 2001; revision received March 19, 2002. Associate Editor: C. Amon.

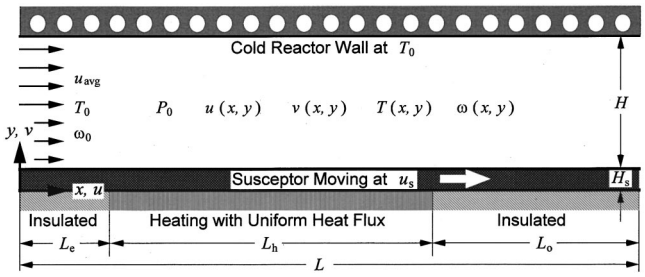

Fig. 1 Schematic of the present continuous chemical vapor deposition system

newly defined parameters, as well as of performance curves expressed as a function of these parameters, are discussed in detail. The optimization of the process in terms of the heat supplied to the system is also addressed.

Analysis

Physical System. The continuous CVD system dealt with in this study is depicted in Fig. 1. It is a horizontal reactor, where a finite thickness susceptor is allowed to move along the bottom wall. The moving finite thickness susceptor models the combination of wafers (or substrates) and a thin conveyor belt carrying compactly placed wafers on it. Continuous deposition processing is made possible by such susceptor motion. Silicon deposition from silane (SiH_4) diluted in hydrogen (H_2) carrier gas is chosen, not only because there have been extensive studies on its chemistry [2,3,14–16], but also because experimental data for model validation are readily available [17].

Gases flow in and out of the reactor at the atmospheric pressure P_0. Note here that continuously moving susceptors are particularly suited for atmospheric reactors due to easier sealing [12,13]. The susceptor moves at a constant speed u_s in the direction of bulk gas flow. The bottom wall consists of three zones: entrance, heating, and outlet, the first and last of which are thermally insulated. A uniform heat flux is supplied to the susceptor through the heating zone, enabling silane to react and deposit silicon onto the surface. The upper reactor wall is composed of silica and mirror-like coating on the outer surface, being radiatively opaque. In order to prevent unwanted deposition, the upper wall is water cooled to the ambient temperature. Due to conduction and heat conveyed by the susceptor motion, chemical vapor deposition can take place all along the reactor length, which makes the length of heating zone an important variable. For a given total heat input, as an example, changes in the length of the heating zone give rise to different temperature profiles, thereby altering the overall growth rates.

The present study focuses primarily on the moving susceptor. All operating conditions and geometric factors, except those relevant to the susceptor, are fixed at typical values [11,17,18]. The reactor channel is taken as 0.02 m high by 0.7 m long ($H \times L$). Gas enters the reactor at the average velocity (u_{avg}) of 0.175 m/s under $P_0 = 1$ atm and $T_0 = 300$ K. The cold wall temperature (T_0) is also set at 300 K. The partial pressure of silane (P_{SiH_4}) at the inlet is taken as 124.1 Pa, from which the inlet mass fraction ω_0 is calculated. A total heat input (Q_t) of 30 kW is chosen so that the susceptor surface temperature attains the experimental conditions in the presence of radiation heat exchange [17]. Finally, the lengths of entrance (L_e) and heating zones (L_h) are taken as 0.1 and 0.3 m, respectively, unless specified otherwise.

Mathematical Model. In horizontal CVD reactors two-dimensional modeling is valid if the channel width-to-height (aspect) ratio is large and forced convection is dominant [19]. For the system under consideration, buoyancy effects were earlier shown to be negligible.[11] Assuming that the present reactor is wide enough, we can employ a two-dimensional model. In describing two-dimensional steady-state transport phenomena occurring in the reactor, some commonly accepted assumptions have been introduced [1–3,14]. The flow is taken as laminar with negligible viscous dissipation effects. Note that the present operating conditions correspond to the Reynolds number of 32 when based on the inlet conditions and channel height. The gases are regarded as ideal and non-participating for thermal radiation. Since silane is highly diluted in a single carrier gas, the dilute mixture approximation can be invoked. It is a known fact that variable property and Soret effects are important in cold wall horizontal CVD reactors [18]. Despite its negligible effect, the buoyancy term is retained for the completeness of modeling.

In order to place the main focus on thermal characteristics associated with the susceptor motion, a simple, lumped overall surface reaction is adopted, precluding complicated gas phase reactions. Although many studies aimed at developing CVD chemistry models for silicon deposition from silane-hydrogen have been carried out, there is no established model that is commonly accepted in this area and many uncertainties are involved in using the different models [14,18]. In conjunction with the present susceptor arrangement, two additional issues need to be considered. One is that radiative loss from the susceptor surface is expected to be a dominant heat transport mode when a prescribed heat flux is imposed from the bottom. The other is that conjugate heat exchange between the susceptor and gas phase may affect the surface temperature at which chemical reaction takes place. For a proper prediction of deposition processes, both of these should be incorporated in the model.

Owing to the dilute mixture approach, the governing equations and boundary conditions are substantially simplified. A single concentration equation is enough to describe mass transfer because silane is the only gas species involved in the reaction. Since general versions of the formulation are available elsewhere [1–3,14], specific equations applicable to the present system are listed in the following:

$$\frac{\partial(\rho u)}{\partial x} + \frac{\partial(\rho v)}{\partial y} = 0 \tag{1}$$

$$\frac{\partial(\rho u \phi)}{\partial x} + \frac{\partial(\rho v \phi)}{\partial y} = \frac{\partial}{\partial x}\left(\Gamma \frac{\partial \phi}{\partial x}\right) + \frac{\partial}{\partial y}\left(\Gamma \frac{\partial \phi}{\partial y}\right) + S_\phi \tag{2}$$

where the general dependent variable ϕ, diffusion coefficient Γ, and source terms S_ϕ are defined as

$$\phi = u, v, T, \text{ and } \omega \tag{3}$$

$$\Gamma = \mu, \mu, k/c_p, \text{ and } \rho D \tag{4}$$

$$S_u = -\frac{\partial P}{\partial x} + \frac{\partial}{\partial x}\left(\mu \frac{\partial u}{\partial x}\right) + \frac{\partial}{\partial y}\left(\mu \frac{\partial v}{\partial x}\right) - \frac{2}{3}\frac{\partial}{\partial x}\left[\mu\left(\frac{\partial u}{\partial x} + \frac{\partial v}{\partial y}\right)\right] \tag{5}$$

$$S_v = -\frac{\partial P}{\partial y} + \frac{\partial}{\partial x}\left(\mu \frac{\partial u}{\partial y}\right) + \frac{\partial}{\partial y}\left(\mu \frac{\partial v}{\partial y}\right) - \frac{2}{3}\frac{\partial}{\partial y}\left[\mu\left(\frac{\partial u}{\partial x} + \frac{\partial v}{\partial y}\right)\right] - \rho g \tag{6}$$

$$S_T = \frac{k}{c_p^2}\left(\frac{\partial T}{\partial x}\frac{\partial c_p}{\partial x} + \frac{\partial T}{\partial y}\frac{\partial c_p}{\partial y}\right) + S_r \tag{7}$$

$$S_\omega = \frac{\partial}{\partial x}\left(D^T \frac{\partial \ln T}{\partial x}\right) + \frac{\partial}{\partial y}\left(D^T \frac{\partial \ln T}{\partial y}\right) \tag{8}$$

While the flow and mass transfer equations are solved in the gas phase only ($H_s \leq y \leq H_s + H$), the energy equation applies to the combined susceptor-gas region ($0 \leq y \leq H_s + H$) to incorporate conjugate heat transfer. The boundary conditions are specified so as to cope with such situations. At the inlet, the flow is assumed to

be fully developed, giving rise to a parabolic profile. The susceptor as well as the gas enter the reactor at the ambient temperature. The flow, temperature, and concentration are regarded as fully developed at the exit, so that zero gradient conditions are applied there. At the susceptor surface, the gas obeys the dilute mixture approximation, and a species balance on silane yields the mass transfer boundary condition. The upper wall is kept cold, and is regarded as impermeable. Those conditions are expressed as follows:

$$u=(6u_{\text{avg}}-3u_s)(\tilde{y}-\tilde{y}^2)+u_s(1-\tilde{y});\quad v=0;\quad T=T_0;$$
$$\omega=\omega_0 \quad \text{at} \quad x=0 \tag{9}$$

$$\frac{\partial u}{\partial x}=0;\quad v=0;\quad \frac{\partial T}{\partial x}=0;\quad \frac{\partial \omega}{\partial x}=0 \quad \text{at} \quad x=L \tag{10}$$

$$u=u_s;\quad v=0;\quad \rho D\frac{\partial \omega}{\partial y}+D^T\frac{\partial \ln T}{\partial y}=M_{\text{SiH}_4}\Re \quad \text{at} \quad y=H_s \tag{11a}$$

$$-k_s\frac{\partial T}{\partial y}=q_w \quad \text{in} \quad L_e<x<L_e+L_h$$
$$\text{and} \quad \frac{\partial T}{\partial y}=0 \quad \text{elsewhere at} \quad y=0 \tag{11b}$$

$$u=0;\quad v=0;\quad T=T_0;\quad \rho D\frac{\partial \omega}{\partial y}+D^T\frac{\partial \ln T}{\partial y}=0 \quad \text{at} \quad u=H_s+H \tag{12}$$

where $\tilde{y}=(y-H_s)/H$ and $q_w=Q_t/L_h$.

Although several sophisticated models for radiation heat transfer in a horizontal CVD reactor have been proposed, e.g., [20,21], a fairly simple one that retains only the basic feature is employed here. Assuming that the inlet and outlet openings are black surfaces at the ambient temperature, the reactor can be treated as an enclosure. The susceptor surface needs to be subdivided due to the nonuniform temperature, whereas each of the other isothermal surfaces is taken as a single area element. Let N be the number of subdivisions in the x-direction, then $N+3$ surface elements constitute the enclosure. Since the gases are nonparticipating, the net-radiation method [22] for an enclosure can be used to obtain the net radiative loss from each surface, for which both the upper reactor wall and the susceptor surface are assumed to be opaque and gray. The energy balance for surface n in terms of radiosity is

$$q_{o,n}+\frac{1-\varepsilon_n}{\varepsilon_n}\sum_{j=1}^{N+3}F_{n-j}(q_{o,n}-q_{o,j})=\sigma T_n^4 \tag{13}$$

Once the radiosity $q_{o,n}$ is known, the net radiative loss $q_{r,n}$ is calculated by

$$q_{r,n}=\frac{1-\varepsilon_n}{\varepsilon_n}(\sigma T_n^4-q_{o,n}) \tag{14}$$

This loss is incorporated into the energy equation via the source term as $S_r=-q_r\times$(radiating area/volume) in every susceptor subdivision located along the surface. Of course, $S_r=0$ elsewhere.

Deposition Model. In the present system, there are large temperature variations along the susceptor surface due to uneven heating, motion, and inlet conditions. This means that the deposition process cannot be simply treated as diffusion-controlled. Although gas phase reactions were excluded, the silane concentration can be influenced by the surface boundary conditions. In view of these factors, it is necessary to adopt an overall surface reaction that depends on the reactant concentration as well as the surface temperature. The mechanism proposed by Claasen et al. [15] and refined later [16] seems to meet the need. Then, the reaction rate is expressed as

$$\Re=\frac{rP_{\text{SiH}_4}}{1+A_1P_{\text{H}_2}+A_2P_{\text{SiH}_4}}[\text{mol}-\text{Si/m}^2\text{s}] \tag{15}$$

where the rate constant is

$$r=1.25\times10^9e^{-18500/T}[\text{mol}-\text{Si/atm m}^2\text{s}] \tag{16}$$

In most of stationary reactors, the deposition characteristics have been represented by the local film growth rate

$$G=(M_{\text{Si}}/\rho_{\text{Si}})\Re \tag{17}$$

This quantity needs to be modified to characterize the performance in continuous processing. A dimensionless average growth rate defined as

$$\eta=\frac{\rho_{\text{Si}}\overline{G}L}{\rho_0u_{\text{avg}}\omega_0H(M_{\text{Si}}/M_{\text{SiH}_4})} \tag{18}$$

can take the place of G. This parameter indicates the ratio of the total deposition rate of silicon along the susceptor to the supply rate at the inlet. From its physical meaning, η can be termed *deposition efficiency*. The species conservation of silicon (or silane) allows us to evaluate it alternatively as [17,23].

$$\eta=1-\frac{\int_{H_s}^{H_s+H}\rho u\omega|_{x=L}dy}{\rho_0u_{\text{avg}}\omega_0H} \tag{19}$$

Since the deposition efficiency includes reactor inlet conditions as well as the film growth rate, it can be used as a general performance index in CVD systems where film uniformity is not a major concern.

Scale Analysis

It would be useful, especially in a complicated system, if we can identify relevant parameters and infer their qualitative effects prior to the detailed study. To this end, a scale analysis for the susceptor energy balance is carried out. This analysis is based on the assumption that the deposition performance depends primarily on the susceptor temperature, being independent of the species concentration. Further assuming constant properties, the energy equation for the moving susceptor can be rewritten as

$$(\rho c_p)_su_s\frac{\partial T_s}{\partial x}=k_s\left(\frac{\partial^2T_s}{\partial x^2}+\frac{\partial^2T_s}{\partial y^2}\right) \tag{20}$$

where the subscript s is used to denote the susceptor. Equation (20) is scaled as

$$\text{Pe}\frac{(\Delta T_s)_x}{L^2}\sim\frac{(\Delta T_s)_x}{L^2}+\frac{(\Delta T_s)_y}{H_s^2} \tag{21}$$

This relation has two limiting cases depending on the magnitude of Pe. From the inlet and outlet boundary conditions, the horizontal temperature difference can be estimated as $(\Delta T_s)_x\sim T_{s,\max}-T_0$. According to the basic assumptions mentioned here, it is deduced that

$$\eta\sim\theta_s=\frac{k_{s,\text{ref}}(T_{s,\max}-T_0)}{q_wL} \tag{22}$$

where the subscript ref designates the reference conditions. the scale of vertical temperature difference can be expressed in terms of the supplied heat flux s $(\Delta T_s)_y\sim q_wH_s/k_s$. Since the analysis procedure is straightforward, only the final results are presented here, i.e.,

$$\eta\sim K^{-1} \quad \text{for} \quad \text{Pe}\ll1 \tag{23}$$

$$\eta\sim S^{-1} \quad \text{for} \quad \text{Pe}\gg1 \tag{24}$$

New dimensionless parameters K and S are defined, respectively, as

$$K = \frac{k_s H_s}{k_{s,\mathrm{ref}} H_{s,\mathrm{ref}}} \tag{25}$$

$$S = \frac{(\rho c_p)_s u_s H_s}{k_{s,\mathrm{ref}}} \tag{26}$$

In view of the fact that Eq. (25) is associated with the longitudinal conduction capability of a susceptor, K is termed *conductance ratio*. Although S physically represents the dimensionless heat capacity rate of a moving susceptor, we simply call it *susceptor parameter*. Since the two parameters are defined in terms of the susceptor thickness, material properties, and speed only, the qualitative relations, Eqs. (23) and (24), remain valid regardless of the change in heat transfer between the susceptor and gas. The effect of conjugate heat transfer would appear through the quantitative dependence of η on K and S.

Although the preceding results need confirmation, it is worth noting their implications briefly at this stage. First of all, the present continuous system may be characterized by the two parameters. The susceptor Peclet number, which appears in the scaling procedure, is irrelevant to the system performance. Next, in each limiting case of Pe the deposition efficiency is expressed in terms of a single parameter. Such a feature may be of practical importance in data reduction. Finally, differently from Eq. (23), the deposition efficiency should approach a finite value as K approaches zero since $\eta < 1$ by definition.

Properties. Using the dilute mixture approximation, it is easy to evaluate both thermophysical and transport properties of gases. Since silane is present in small fractions, properties of the mixture are taken as those of the hydrogen carrier gas. The properties are allowed to vary with temperature as [11,18,24,25]

$$\rho = P_0 M_{\mathrm{H}_2} / (\mathbf{R} T) \tag{27}$$

$$c_p = 1.44 \times 10^4 - 2.61 \times 10^{-1} T + 8.67 \times 10^{-4} T^2 \tag{28}$$

$$\mu = \mu_0 (T/T_0)^{0.648} \tag{29}$$

$$k = k_0 (T/T_0)^{0.691} \tag{30}$$

where $\mu_0 = 8.96 \times 10^{-6}$ kg/ms and $k_0 = 1.83 \times 10^{-1}$ W/mk. The power-law dependence is also used for the binary diffusion coefficient of SiH_4–H_2 mixture

$$D = D_0 (T/T_0)^{1.70} \tag{31}$$

where $D_0 = 6.24 \times 10^{-5}$ m^2/s. For a dilute mixture, the thermal diffusion coefficient can be expressed as

$$D^T = \rho D a \omega \tag{32}$$

The factor a is estimated using the Holstein's approximation [26] and curve-fitted Lennard-Jones parameters [27].

The density of silicon is taken as $\rho_{\mathrm{Si}} = 2330$ kg/m^3. In response to the result of scale analysis, a set of reference conditions for the susceptor are chosen based on the previous work [11] as: $H_{s,\mathrm{ref}} = 2$ mm, $(\rho c_p)_{s,\mathrm{ref}} = 1.631 \times 10^6$ J/m^{3}K, and $k_{s,\mathrm{ref}} = 141.2$ W/mK. Noting that the actual susceptor is a composite element (of conveyor belt and silicon wafer), its properties do not necessarily correspond to a specific material. The susceptor properties may have wide spectra and vary diversely with temperature depending on the material combination. Their effects on the deposition process can be assessed by a parametric study as is done in this work. Those values listed here were taken for silicon at the ambient temperature as an approximation. Other numerical data used here include well-known universal constants and molecular masses, which can be found elsewhere. In view of the previous work [24], emissivities of the upper wall and susceptor surfaces are taken as 0.7 and 0.6, respectively. For the same reason as mentioned earlier, the temperature dependence of emissivity is not taken into account.

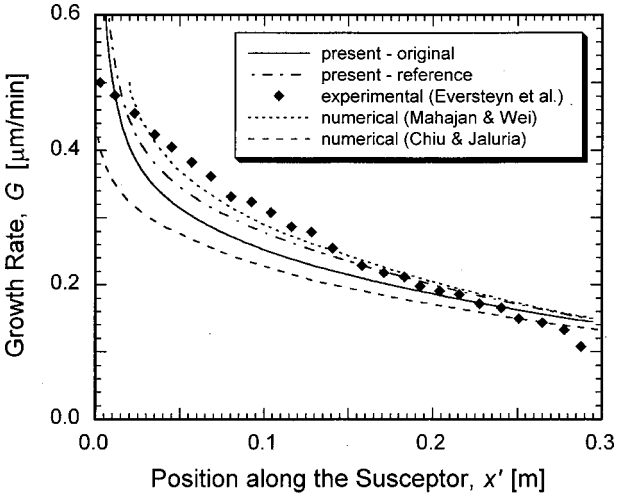

Fig. 2 Comparison of the predicted film growth rate with existing experimental data [17] and numerical results [11,18]

Numerical Method. The governing equations and boundary conditions are discretized on a nonuniform staggered grid system using a finite volume method. In correcting the pressure field, an approach similar to the SIMPLE algorithm [28] has been employed. As noted earlier, the same energy equation covers the combined susceptor-gas region along with individual property values, yielding the conjugate temperature field. Since the species conservation equation is decoupled from the others under the dilute mixture approximation, it is solved after the flow and temperature fields have converged.

A typical grid system consists of 450 streamwise and 40 transverse nodes in the gas phase. The number of transverse nodes in the susceptor material depends on the thickness considered. For a typical case of $H_s = 2$ mm, 10 nodes are used. The grid size was chosen by appropriate grid refinement so that the converged solutions are independent of the grid. It is also confirmed that the numerical results are independent of other user-specified variables such as the initial guess and convergence criteria.

Results and Discussion

A large number of simulations have been performed to investigate the influences of susceptor-related factors. The simulated cases are divided into four groups according to the susceptor material and thickness. Case A just refers to the reference conditions. Each of Cases B, C, and D designates the change in k_s, H_s, and both of k_s and H_s, respectively, while the other variables remain at the reference values.

Model Validation. In order to validate the present numerical model, two sets of the predicted local growth rate of silicon film are compared in Fig. 2 with the well-known experimental data of Eversteyn et al. [17]. For comparative discussions, the plot also includes two representative numerical results [11,18] that commonly employed two-dimensional models. A stationary, isothermal susceptor at 1323 K is used for this comparison to replicate the experimental conditions. The susceptor in Fig. 2 corresponds to the heating zone in Fig. 1. Hence, $x' = x - L_e$. One of the present predictions, the solid curve, is referred to as original because it is obtained from the model without any change. The other is a reference case for later discussion.

Except near the leading edge, the present simulation favorably (within 20 percent bound) agrees with the experimental data. The leading edge discrepancy seems to originate not from improper modeling but from mismatch in the boundary conditions between the prediction and the experiment. A steep drop in the growth rate always appears in numerical predictions employing an isothermal

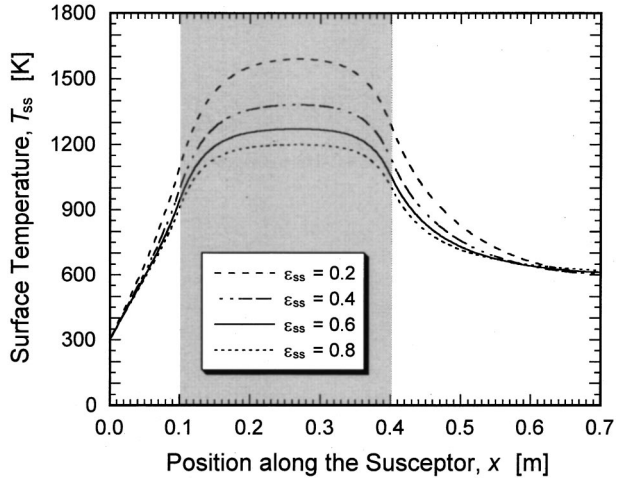

Fig. 3 Effect of the susceptor surface emissivity on the temperature distribution

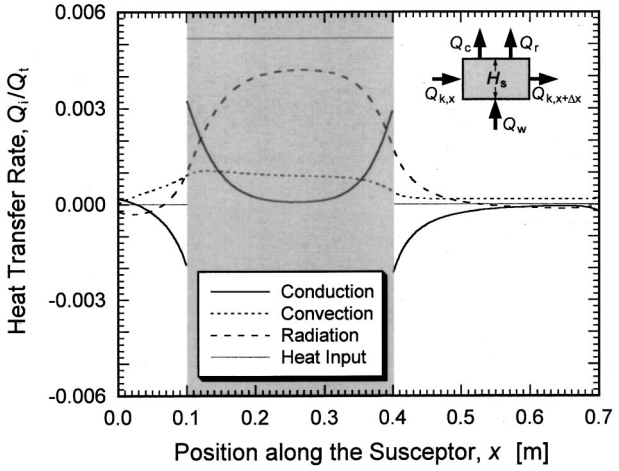

Fig. 4 A typical result of the conjugate heat transfer analysis: heat transport modes for a susceptor segment

susceptor because silane is depleted sharply from the inlet condition to a very low level there. The other numerical results confirm this aspect. In the experiment, the surface temperature at the leading and trailing edges would be lower than specified, deviating from the isothermal condition. A gradual change at the leading edge and inflective decrease at the trailing edge in the experimental growth rate support this arguement.

Regardless of models, all the numerical predictions show the same qualitative trend over the susceptor length. In terms of quantitative agreement with the experiment [17], the original curve of the present prediction appears to be inferior to the result of Mahajan and Wei [18], whereas superior to that of Chiu and Jaluria [11]. This observation, however, needs some explanations. Mahajan and Wei [18] used a larger diffusion coefficient than Eq. (31) and other studies [2,3,24], and assumed the diffusion-controlled deposition. Both of these effects are known to increase the local growth rate. Using their diffusion coefficient in the present model indeed yielded considerably higher growth rates, which are depicted as the reference case in Fig. 2. It is also known [11] that the diffusion-controlled assumption leads to faster film growth than the present reaction kinetics, Eq. (15). Note that the infinite reaction rate is just a limiting case. These facts imply that under proper conditions, the predictions might deviate farther from the experiment than seen here. Meanwhile, Chiu and Jaluria [11] neglected thermal diffusion that acts as obstructing film deposition in silane-hydrogen system. The inclusion of thermal diffusion in their model may produce lower growth rates than the plotted result. It is deduced from this discussion that the present model is capable of resolving the basic characteristics of silicon deposition occurring in a cold wall horizontal CVD reactor within a reasonable tolerance.

Radiation and Conjugate Heat Transfer. In view of their contributions, radiation and conjugate heat transfer in the present continuous system are addressed first. Results are obtained for the case of a stationary susceptor. Figure 3 demonstrates the effect of emissivity on the temperature distribution along the susceptor surface. The shaded areas in Fig. 3 and plots presented from now on indicate the part of susceptor that overlies the heating zone. Over a wide band of the susceptor surface emissivity, the curves show a similar pattern, but temperature differences among them along the heating zone are quite large. Noting that the surface temperature directly affects the deposition rates, the large differences suffice to illustrate the importance of radiation. The radiation model can also be used in reactor design to calculate the total heat input that is needed to maintain a prescribed susceptor temperature. In all the subsequent simulations, the susceptor surface emissivity is set at the previously noted value of 0.6.

The role of radiation can also be understood in Fig. 4, where a typical result of the conjugate heat transfer analysis is depicted. This is the energy balance for a susceptor segment shown in the inset of Fig. 4. Four curves represent net conduction ($Q_{k,x+\Delta x} - Q_{k,x}$), convection ($Q_c$), net radiation ($Q_r$), and heat input ($Q_w$), respectively. The heat input is $q_w \Delta x$ for a segment on the heating zone and 0 elsewhere. It is confirmed that radiation is the dominant heat transfer mode along the susceptor in the heating zone. Two discontinuities in the net conduction curve, which appear at the borders of the heating zone, correspond to each of inflexion points in the temperature distribution (see Fig. 3). Heat conduction through a thin susceptor contributes to smoothen the horizontal temperature variation. Although convection from the susceptor surface to the gas is much smaller than radiation, it may affect the deposition performance when gas phase reactions are included in the model.

Effect of Conductance Ratio. The scale analysis yielded a relation between the deposition efficiency and conductance ratio for small Peclet numbers. Its validity and utility is examined for $S=0$ because a stationary susceptor best satisfies the limiting condition of $\mathrm{Pe} \ll 1$. The local growth rates for two cases with the same value of K, but obtained from different combinations of k_s and H_s, are compared in Fig. 5. For each of $K=1/4$ and 4, Case B and C yield an identical curve despite the physical difference between them. Such indiscernible agreements appear in all other results, which confirm that the conductance ratio is indeed a characteristic parameter. On the other hand, the difference in pattern among cures that correspond to three values of K indicates that the conductance ratio may affect the overall deposition behavior.

Figure 6 delineates the stationary deposition efficiency calculated over a wide range of K and for as many combinations of k_s and H_s as possible. Cases B, C, and D with the same K are reduced to a single value of η_{st}, within a bound of numerical truncation. Although the η_{st} curve does not fit the scale relation, Eq. (23), the two results show a similar trend in that they decrease toward zero as K increases. At small values of K, however, the curve deviates far from the relation, as noted before. With decreasing the conductance ratio, the curve approaches asymptotically to the deposition efficiency for $K \to 0$. Noting that that variation of η_{st} is steep in a narrow band of K (e.g., $0.1 < \eta_{st} < 0.5$ for $1 < K < 10$), the overall deposition performance may depend

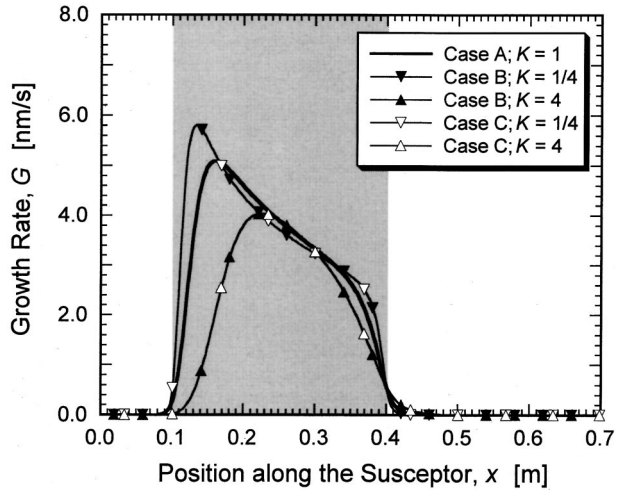

Fig. 5 Spatial variations of the film growth rate for different values and combinations of conductance ratio

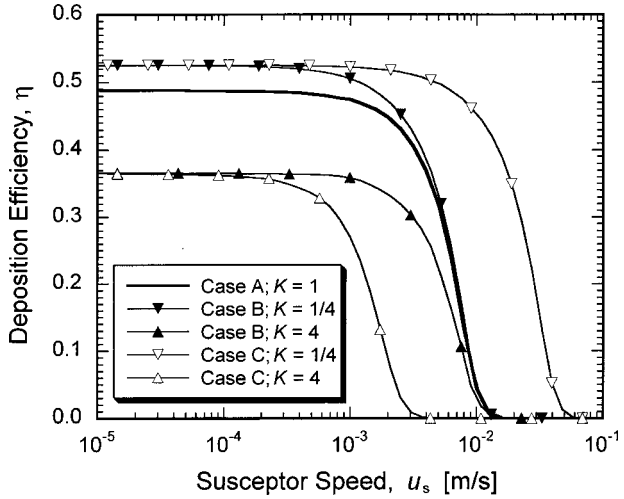

Fig. 7 Dependence of the deposition efficiency on the susceptor speed for different values and combinations of conductance ratio

strongly on the selection of susceptor. From Figs. 5 and 6, along with Eq. (23), it is evident that the conductance ratio is the only parameter representing a stationary system.

Although not shown here, the susceptor temperature over the heating zone, which primarily affects the deposition rate, decreases with increasing K, leading to the pattern of Fig. 6. The $\eta_{st}-K$ plot can be used either to estimate the deposition efficiency for a given susceptor or to select the susceptor material and thickness that meet a prescribed performance criterion.

Susceptor Speed. In the present continuous system, the susceptor speed is of fundamental importance. The deposition efficiency is readily expected to decrease as the speed increases. In order to quantify the effect of susceptor speed, η is plotted as a function of u_s in Fig. 7 for the same values of K and combinations of k_s and H_s as in Fig. 5. Regardless of the value of K, all curves show a similar pattern. As u_s increases, η is at first constant, then decreases gradually, and finally decreases sharply, approaching smoothly to zero. In the region of large u_s, on the other hand, the behavior of η is affected by both the value of K and the combination of properties used to obtain a given value. The relation between η and u_s is independent of k_s, but dependent on H_s. Such dependence is consistent with the results of scale analysis, Eqs. (24) and (26), which enable us to deduce that the deposition efficiency can be characterized by the susceptor parameter only.

When the speed u_s is converted into the susceptor parameter S according to the definition given in Eq. (26), the efficiency curves with the same value of K nearly coincide with each other. The curves for different values of K disagree with one another due to the difference in η_{st}. This problem can be resolved by normalizing η by η_{st}. Figure 8 depicts the reduced result, i.e., the relation between the normalized efficiency and susceptor parameter, for which the data are taken from Fig. 7. Although each set of data differs a little from one another, the deviations seem to be small enough to call the result a single curve. Additional calculations for the wide range of K (as in Fig. 6) and various combinations of $(\rho c_p)_s u_s$ yield the same curve. A decrease in η/η_{st} over the region of large S, where $\mathrm{Pe}\ll 1$, qualitatively agrees with the scale relation, Eq. (24). From an engineering viewpoint, this curve along with Fig. 6 can be used for susceptor design. Under the present conditions, the deposition efficiency is readily obtained for any combinations of susceptor material, thickness, and speed through a simple procedure. Once K and S are known, η_{st} and η/η_{st} can be read in Figs. 6 and 8, respectively. Multiplying them produces the required η. Therefore, with these plots, we can avoid

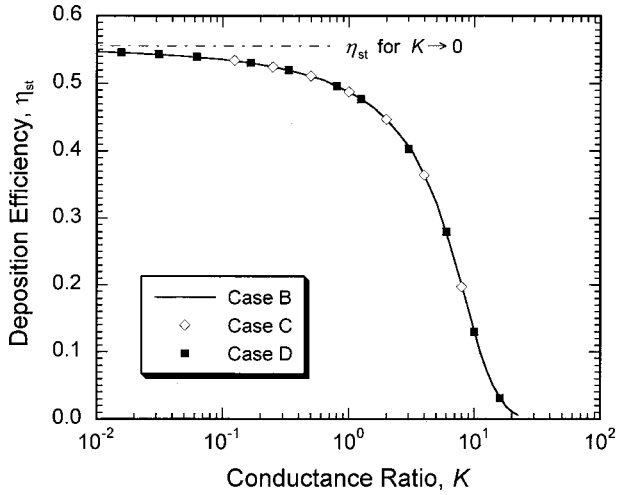

Fig. 6 Dependence of the stationary deposition efficiency on conductance ratio

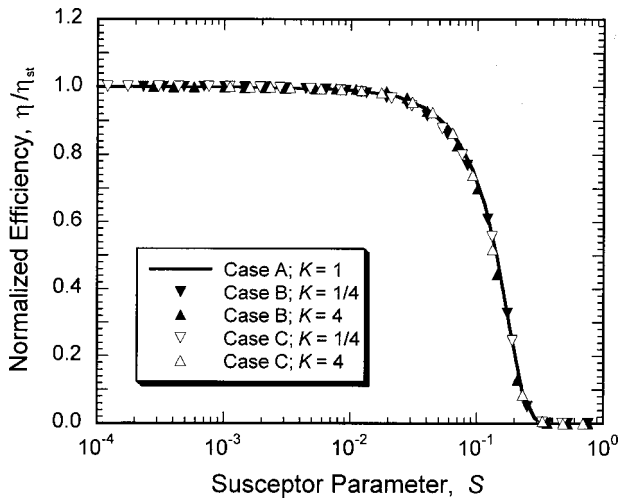

Fig. 8 Dependence of the normalized deposition efficiency on susceptor parameter

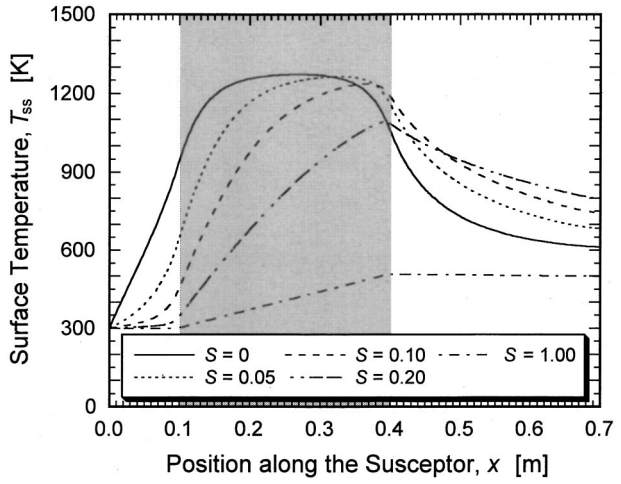

Fig. 9 Effect of susceptor parameter on the temperature distribution along the susceptor surface

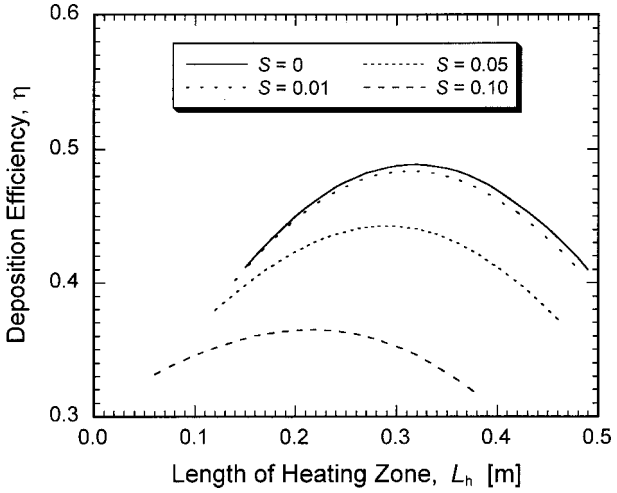

Fig. 11 Deposition efficiency as a function of heating zone length at four selected values of susceptor parameter

design conditions that result in low efficiencies. In this sense, the two curves comprise performance curves for the present continuous system.

The effect of susceptor speed on the local behavior is briefly reported here. Figure 9 presents the temperature distributions along the susceptor surface for five values of S. With increasing S (or equivalent u_s), a high temperature band narrows, the maximum value lowers and shifts downstream toward the end of heating zone, and the profile eventually becomes linear. Heat conveyed by the susceptor movement is responsible for those changes, which in turn leads to the trends seen in Fig. 8. It is unlikely that a value of S higher than 0.1 will be adopted in the design of practical systems.

Length of Heating Zone. For a given total heat input, the length of heating zone directly affects the temperature profile due to $q_w = Q_t / L_h$. The effect on the deposition performance for representative values of K and S is investigated. Figure 10 illustrates the dependence of η_{st} on L_h at four selected values of K for $S = 0$. For each K, there exists an optimum length of heating zone that maximizes the deposition efficiency. The reason is clear when we consider two limiting cases: $L_h \to 0$ and $L_h \to L$. When L_h is short, the susceptor temperature on the heating zone tends to rise high due to intensive heating, which in turn induces a large radiative loss from the surface. Although the temperature is still high, the average deposition rate becomes low because of a short deposition length. When L_h is long, the susceptor temperature becomes low, thereby heat losses being reduced. Such moderate temperature is ineffective for chemical reaction, decreasing the deposition efficiency. The optimum length $L_{h,\mathrm{opt}}$ shortens as K increases. Conduction through the susceptor is enhanced with increasing K, so that intensive heating is more effective for raising the surface temperature high enough for deposition. If conduction is suppressed with decreasing K, extensive heating yields a longer effective deposition length. A short L_h along with small K leads to a large radiative loss. This is why η_{st} for a small K decreases more sharply from the maximum on the short L_h side than on the large one.

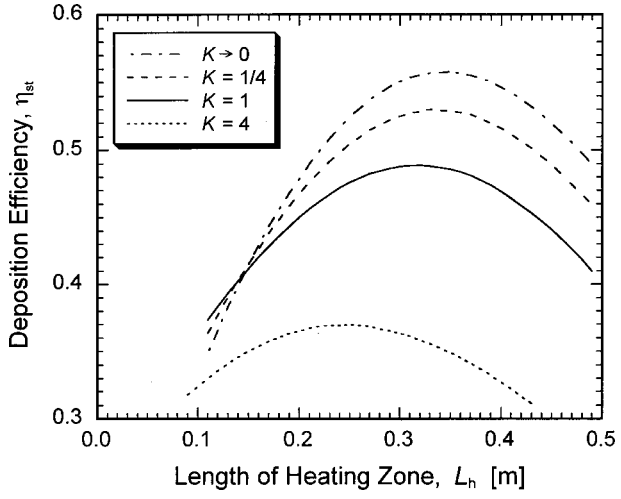

Fig. 10 Stationary deposition efficiency as a function of heating zone length at four selected values of conductance ratio

Another result is the dependence of η on L_h at representative values of S for $K = 1$, as depicted in Fig. 11. The overall picture looks similar to Fig. 10. Each curve shows an increasing-decreasing pattern, encompassing the local maximum point. The optimum length of the heating zone also shortens as S increases. The influence of S on $L_{h,\mathrm{opt}}$, however, is caused by a different mechanism from that of K. With increasing S, the width of the susceptor at high temperature narrows and the surface temperature decreases (see Fig. 9). This means that more intensive heating is needed to raise the temperature high enough for deposition. It is worth noting that the variation band of $L_{h,\mathrm{opt}}$ in both of Figs. 10 and 11 is relatively narrow. The value $L_h = 0.3$ m used so far is close to $L_{h,\mathrm{opt}}$ for a wide range of K and S. Because of the convex shape of the efficiency curve, a single value of η, other than at the maximum, corresponds to two different lengths: one is shorter, and the other longer than $L_{h,\mathrm{opt}}$. The shorter one is preferable because a smaller reactor is desirable. Other factors, such as microstructure of deposited film, conveyor drive system, and wafer loading, should be taken into account in the actual design.

In summary, the dependence of deposition performance on the length of heating zone stems from how the supplied heat is distributed along the susceptor and transported to the surroundings. Since the parameters K and S affect the distribution and transport, the efficiency curve depends on both of them. It is obvious that the radiation and conjugate heat transfer play key roles in quantifying such effects in deposition characteristics.

Conclusions

A systematic study has been carried out to investigate the performance characteristics of continuous chemical vapor deposition of silicon in a horizontal cold wall reactor, in which the main focus is placed on a moving finite thickness susceptor. The nu-

merical model used for simulation accounts for temperature-dependent properties, thermal diffusion, radiation among surfaces, and conjugate heat transfer between the susceptor and gas. The validity and capability of the model have been confirmed by a reasonably good agreement between the predicted result and available experimental data, and a fine resolution of the coupled heat transfer. Scale analysis for the moving susceptor yield two characteristic parameters and a pair of qualitative relations, which prove to be useful for understanding the deposition behavior and analyzing the predicted data.

When the susceptor is motionless, the stationary deposition efficiency is determined by the conductance ratio only. The efficiency curve monotonically decreases that for the thin susceptor limit to zero as the conductance ratio increases. When the susceptor is in motion, the deposition efficiency, normalized by the value under stationary state conditions, is a function of the susceptor parameter only. With increasing the susceptor parameter (or speed), the normalized efficiency curve remains almost unity and then decreases sharply toward zero. This variation demonstrates the feasibility of continuous processing in that the susceptor can move up to considerable speed without sacrificing deposition efficiency. Since these two curves represent the performance characteristics of a continuous system, they can be used to determine the susceptor material, thickness, or moving speed in the design of practical systems. Finally, an optimum length of heating zone that maximizes the deposition efficiency always exists under a fixed total heat input and depends on the characteristic parameters. Adjusting the length of the heating zone, along with the use of the performance curves, can play an important role in improving the deposition efficiency of continuous CVD systems.

Acknowledgments

This work was conducted during the first author's (H.Y.) sabbatical leave. He would like to acknowledge the financial support provided by the Korea Research Foundation under Grant Number KRF-2000-EA0005 and the visiting position furnished by Rutgers University. The partial support from NSF under Grant Number DMI-96-33194 is also acknowledged.

Nomenclature

A_1 = constant in Eq. (15), $A_1 = 1.75 \times 10^3$ atm^{-1}
A_2 = constant in Eq. (15), $A_2 = 4.00 \times 10^4$ atm^{-1}
a = thermal diffusion factor
c_p = specific heat
D = binary diffusion coefficient
D^T = thermal diffusion coefficient
F = configuration factor
$\underline{G}$ = local film growth rate
G = average growth rate, $\frac{1}{L}\int_0^L G(x)dx$
g = magnitude of gravitational acceleration
H = height of reactor
H_s = susceptor thickness
K = conductance ratio
k = thermal conductivity
L = reacator length
L_e, L_h, L_o = length of entrance, heating, and outlet zones
M = molecular mass
N = number of control volumes in the x-direction
P = pressure
P_i = partial pressure of species i
Pe = Peclet number, $(\rho c_p)_s u_s L/k_s$
Q = heat transfer rate
q = heat flux
q_o = radiosity
$\mathbf{R}$ = universal gas constant
$\Re$ = chemical reaction rate
r = reaction rate constant
S = susceptor parameter or source term
T = temperature
u,v = velocity components in x, y-directions
u_{avg} = average gas velocity at the inlet
x, y = coordinates

Greek Letters

ε = emissivity
ϕ = stands for u, v, T, and ω
η = deposition efficiency
μ = viscosity
ρ = density
σ = Stefan-Boltzmann constant
θ = dimensionless temperature
ω = mass fraction of silane

Subscripts

0 = inlet or reference state
c = convection
k = conduction
r = radiation
ref = reference conditions
ss = susceptor surface
st = stationary susceptor
t = total
w = bottom wall

References

[1] Jensen, K. F., Einset, E. O., and Fotiadis, D. I., 1991, "Flow Phenomena in Chemical Vapor Deposition of Thin Films," Annu. Rev. Fluid Mech., **23**, pp. 197–232.
[2] Kleijn, C. R., 1995, "Chemical Vapor Deposition Processes," *Computational Modeling in Semiconductor Processing*, M. Meyyappan, ed., Artech House, Boston, pp. 97–229.
[3] Mahajan, R. L., 1996, "Transport Phenomena in Chemical Vapor-Deposition Systems," Adv. Heat Transfer, **28**, pp. 339–425.
[4] Yamaji, T., Abe, M., Takada, Y., Okada, K., and Hiratani, T., 1994, "Magnetic Properties and Workability of 6.5% Silicon Steel Sheet Manufactured in Continuous CVD Siliconizing Line," J. Magn. Magn. Mater., **133**, pp. 187–189.
[5] Stevenson, P., and Matthews, A., 1995, "PVD Equipment Design: Concepts for Increased Production Throughput," Surf. Coat. Technol., **74–75**, pp. 770–780.
[6] Onabe, K., Kohno, O., Nagaya, S., Shimonosono, T., Iijima, Y., Sadakata, N., and Saito, T., 1996, "Structure and Property of $YBa_2Cu_3O_x$ Tapes Formed on Metallic Substrate by CVD Technique," Mater. Trans., JIM, **37**, pp. 893–897.
[7] Gordon, R., 1997, "Chemical Vapor Deposition of Coatings on Glass," J. Non-Cryst. Solids, **218**, pp. 81–91.
[8] Bansal, N., and Dickerson, R. M., 1997, "Tensile Strength and Microstructural Characterization of HPZ Ceramic Fiber," Mat. Sci. Technol., **A222**, pp. 149–157.
[9] Lackey, W. J., Vaidyaraman, S., Beckloff, B. N., Moss, III, T. S., and Lewis, J. S., 1998, "Mass Transfer and Kinetics of the Chemical Vapor Deposition of SiC onto Fiber," J. Mater. Res., **13**, pp. 2251–2261.
[10] Chiu, W. K. S., and Jaluria, Y., 1999, "Effect of Buoyancy, Susceptor Motion, and Conjugate Transport in Chemical Vapor Deposition Systems," ASME Heat Transfer, **121**, pp. 757–761.
[11] Chiu, W. K. S., and Jaluria, Y., 2000, "Continuous Chemical Vapor Deposition Processing with a Moving Finite Thickness Susceptor," J. Mater. Res., **15**, pp. 317–328.
[12] Dobkin, D. M., 2000, "Injector-based Atmospheric Pressure Reactors," http://www.batnet.com/enigmatics/semiconductor_processing/CVD_Fundamentals/reactors/APCVD_ovvu.html.
[13] Silicon Valley Group, Inc., 2000, Annual Report, Securities Exch. Comm., http://www.asml.com/investors/pdf/annual_report_svg00.pdf, p. 7.
[14] Kleijn, C. R., 2000, "Computational Modeling of Transport Phenomena and Detailed Chemistry in Chemical Vapor Deposition—A Benchmark Solution," Thin Solid Films, **365**, pp. 294–306.
[15] Claasen, W. A. P., Bloem, J., Valkenburg, W. G. J. N., and van den Brekel, C. H. J., 1982, "The Deposition of Silicon from Silane in a Low-Pressure, Hot-Wall System," J. Cryst. Growth, **57**, pp. 259–266.
[16] Jensen, K. F., and Graves, D. B., 1983, "Modeling and Analysis of Low Pressure CVD Reactors," J. Electrochem. Soc., **120**, pp. 1950–1957.
[17] Eversteyn, F. C., Severin, P. J. W., van den Brekel, C. H. J., and Peek, H. L., 1970, "A Stagnant Layer Model for the Epitaxial Growth of Silicon from Silane on a Horizontal Reactor," J. Electrochem. Soc., **117**, pp. 925–931.
[18] Mahajan, R. L., and Wei, C., 1991, "Buoyancy, Soret, Dufour, and Variable Property Effects in Silicon Epitaxy," ASME Heat Transfer, **113**, pp. 688–695.
[19] Quazzani, J., Chiu, K.-C.,and Rosenberger, F., 1988, "On the 2D Modeling of Horizontal CVD Reactors and its Limitations," J. Cryst. Growth, **91**, pp. 497–508.
[20] Chinoy, P. B., Kaminski, D. A., and Ghandhi, S. K., 1991, "Effects of Thermal

Radiation on Momentum, Heat, and Mass Transfer in a Horizontal Chemical Vapor Deposition Reactor,'' Numer. Heat Transfer, Part A, **19**, pp. 85–100.
[21] Kadinski, L., Makarov, Yu N., Schaefer, M., Vasil'ev, M. G., and Yuferev, V. S., 1995, ''Development of Advanced Mathematical Models for Numerical Calculations of Radiative Heat Transfer in Metalorganic Chemical Vapor Deposition Reactors,'' J. Cryst. Growth, **146**, pp. 209–213.
[22] Siegel, R., and Howell, J. R., 1992, *Thermal Radiation Heat Transfer*, 3rd ed., Hemisphere Publishing Corp., Washington, D.C.
[23] Tsai, H. C., Greif, R., and Joh, S., 1995, ''A Study of Thermophoretic Transport in a Reacting Flow with Application to External Chemical Vapor Deposition Processes,'' Int. J. Heat Mass Transf., **38**, pp. 1901–1910.
[24] Kleijn, C. R., and Hoogendoorn, C. J., 1991, ''A Study of 2- and 3-D Transport Phenomena in Horizontal Chemical Vapor Deposition Reactors,'' Chem. Eng. Sci., **46**, pp. 321–334.
[25] Moffat, H. K., and Jensen, K. F., 1988, ''Three-Dimensional Flow Effects in Silicon CVD in Horizontal Reactors,'' J. Electrochem. Soc., **135**, pp. 459–471.
[26] Holstein, W. L., 1988, ''Thermal Diffusion in Metal-Organic Chemical Vapor Deposition,'' J. Electrochem. Soc., **135**, pp. 1788–1793.
[27] Neufeld, P., Janzen, A. R., and Aziz, R. A., 1972, ''Empirical Equations to Calculate 16 of the Transport Collision Integrals $\Omega^{(l,s)*}$ for the Lennard-Jones (12-6) Potential,'' J. Chem. Phys., **57**, pp. 1100–1102.
[28] Patankar, S. V., 1980, *Numerical Heat Transfer and Fluid Flow*, Hemisphere Publishing Corp., New York.